

1

Introduction to Zinc–Air Batteries

Qian Lu¹, Xiaohong Zou², and Yunfei Bu¹

¹Nanjing University of Information Science and Technology, Jiangsu Collaborative Innovation Center of Atmospheric Environment and Equipment Technology, Jiangsu Key Laboratory of Atmospheric Environment Monitoring and Pollution Control, UNIST-NUIST Environment and Energy Jointed Lab, School of Environmental Science and Technology, No. 219 Ningliu Road, Nanjing 210044, P. R. China

²Nanjing Tech University, Jiangsu National Synergetic Innovation Center for Advanced Materials (SICAM), State Key Laboratory of Materials-Oriented Chemical Engineering, College of Chemical Engineering, No. 30 South Puzhu Road, Nanjing 211816, P. R. China

1.1 Introduction

With the rapid development of society, people's dependence on energy sources is increased continually in terms of daily life and transportation [1]. Up to now, nonrenewable energies, such as fossil energy (oil, natural gas, and coal) and nuclear energy, account for 80% of energy consumption, thus inevitably causing serious environmental pollution (green-house gas, SO₂, and NO_x) and rapid consumption of reserve resources [2]. Therefore, it is urgent to develop renewable clean energy, including solar energy, tidal energy, wind energy, and hydropower, to substitute for traditional fossil energy in power grid [3, 4]. Generally, this renewable energy is regarded as intermittent energy, which is highly dependent on resource conditions, such as season, climate, and region; so, we should pay more attention to efficient energy storage and conversion technology to achieve continuous energy output.

Among the numerous energy storage and conversion devices, electrochemical storage and conversion systems, such as Li-ion/nickel-metal hydride (NIMH)/lead–acid battery, Li–sulfur battery, and metal–air battery, show the advantages of high-energy-conversion efficiency and high-energy density [5]. Devices using Li-ion/NIMH/lead–acid batteries as power sources can be seen everywhere in daily life, including mobile phones, laptops, unmanned aerial vehicles, wireless headphones, and even electronic vehicles. Given the great impact of Li-ion batteries on the whole society, the 2019 Nobel Prize in chemistry was awarded to three pioneers, including John B Goodenough, M. Stanley Whittingham, and Akira Yoshino, owing to their great achievement in rechargeable Li-ion batteries [6]. Although Li-ion battery has achieved great success, the low-energy-storage density, high cost, limited reserves of lithium, and insufficient safety for the usage of volatile organic electrolyte remain the biggest headaches in the field of electric vehicles or other

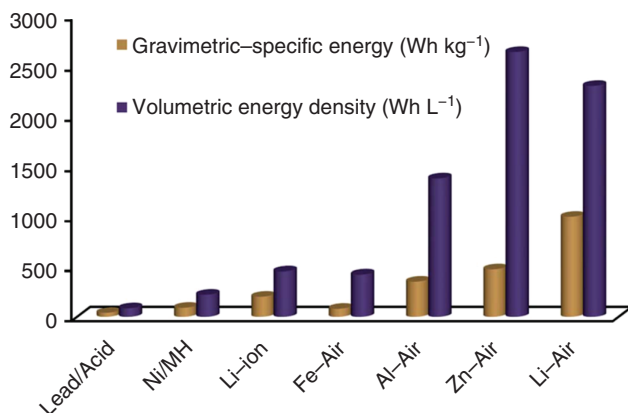


Figure 1.1 The gravimetric and volumetric energy density of various types of secondary batteries. Source: Lee et al. [11]/Reproduced with permission of Royal Society of Chemistry.

portable devices [7, 8]. Therefore, it is imperative to develop other rechargeable batteries with safety, high-specific-energy density, and cost-efficient, such as Li–sulfur battery, metal–air battery, and solid-state Li–metal battery. Among these batteries, metal–air battery is regarded as the next-generation energy-storage system owing to the low cost and high-energy density, while Li–sulfur battery and solid-state Li–metal battery just exhibit the advantage of high-energy density [9, 10]. As shown in Figure 1.1, the gravimetric and volumetric energy density of metal–air batteries, including lithium (Li), zinc (Zn), aluminum (Al), and iron (Fe), are significantly higher than other conventional rechargeable batteries [11, 12]. Although Li–air battery shows the highest theoretical energy density of 3458 Wh kg^{-1} , unfortunately, the volatilization of organic electrolyte and instability of lithium metal, when exposed to oxygen or water, were encountered for Li–air battery with open system, thus causing poor cycle stability [13]. For Fe–air and Al–air batteries, its actual specific energy and energy density are considerably lower than the theoretical value owing to large polarization voltage, its rechargeability is relatively poor in alkaline conditions, and rapid self-discharge through hydrogen-evolution reaction is encountered in alkaline conditions [14, 15]. In contrast, Zn–air battery shows obvious advantages for practical application [16], including (i) actual energy density reaching up to $500\text{--}600 \text{ Wh kg}^{-1}$ (theoretical energy density of 1086 Wh kg^{-1}), which is twofold of advanced lithium-ion batteries; (ii) the discharge platform is extremely stable, which could achieve stable output voltage; (iii) the battery with aqueous electrolyte is safe and environment-friendly; (iv) the cost of Zn–air batteries was decreased by using the zinc metal which is abundant reserves and low cost [16]. Up to now, Zn–air battery has been successfully applied to hearing aid, urban sightseeing vehicles, and postal vehicles. To accelerate and standardize the application of Zn–air batteries in electric vehicles, the Ministry of Industry and Information Technology of China has also approved the “The industry standard of Zn–air battery for electric vehicles” (GB/T 18333.2-2015).

1.2 History of Zn–Air Batteries

The first battery with zinc metal as the anode was developed by Volta in 1796 [17]. In the early nineteenth century, the zinc metal and MnO_2 were applied as the anode and cathode for zinc–manganese dry battery, respectively, with the shape of beaker, while the hybrid NH_4Cl and ZnCl_2 were served as the electrolyte [18]. Based on this, Maiche developed the first primary model of Zn–air battery in 1878 by replacing the MnO_2 with platinum-loaded porous carbon, indicating the first appearance of zinc–air battery [19]. Owing to the usage of weak acid NH_4Cl aqueous solution as electrolyte, the output-discharge current density for this primary zinc–air battery is just 0.3 mA cm^{-2} . Few years later, a Walker–Wilkins battery with first reported gas-diffusion layer consisting of porous carbon black was further designed [20]. In the Walker–Wilkins battery, aqueous potassium hydroxide and nickel were employed as electrolyte and current collectors of the gas-diffusion layer, respectively. At that time, the atmospheric oxygen was identified as the reactant for oxygen-reduction reaction (ORR). In 1932, Heise and Schumadcher redesign a waterproof porous carbon as the air cathode and a NaOH aqueous solution with 20% concentration as the electrolyte [21]. As a result, this Zn–air battery could achieve high-discharge current density of 10 mA cm^{-2} , which marks its practical commercial applications in many fields, including railway signaling equipment and lighthouse. Since the 1970s, the primary coin-type Zn–air battery with low-power density is widely applied in hearing aids, revealing the Zn–air battery entered into our daily life [22]. With rapid development of high-efficient gas-diffusion layer, Zn–air batteries have made great progress in discharge current density reaching up to 1000 mA cm^{-2} in pure oxygen atmosphere, while the electrode thickness was just 0.12–0.5 mm [23]. The high-power density of Zn–air batteries shows application prospects in the field of electric vehicles.

When operating in air atmosphere, the alkaline electrolyte would react with CO_2 to form the solid K_2CO_3 , which could block the gas-diffusion layer [24]. Different from alkaline electrolyte, neutral solution with NH_4Cl as the solute could avoid the direct reaction between alkaline and CO_2 in air to form the carbonates. Until 1973, Jindra et al. found that 5 M NH_4Cl aqueous solution could serve as a quasi-neutral electrolyte to achieve sufficient buffering capacity for primary Zn–air battery [25]. However, the ionic conductivity of neutral electrolyte is relatively poor, thus the Zn–air battery with neutral electrolyte shows low-power density. Alkaline electrolytes (e.g. KOH , NaOH , and LiOH aqueous solutions), which are widely applied in commercial primary Zn–air batteries, are the essential component to achieve high-energy density and power density owing to their high ionic conductivity and high catalytic activity of ORR [26]. For example, the KOH aqueous solution with mass concentration of 35% shows high ionic conductivity of 0.55 S cm^{-1} and low viscosity of 2.2339 mPa s at 25°C , which could provide excellent electrochemical kinetics and mass transfer for Zn–air battery [27]. More importantly, the catalytic activities of ORR and oxygen-evolution reaction (OER) in alkaline electrolytes is evidently better than that in neutral electrolytes.

Above researches about pristine Zn–air batteries just focus on the discharge performance. From 1997 onwards, rechargeable Zn–air batteries with alkaline electrolytes came into sight by researchers [28]. Commonly, 6 M KOH mixed with 0.2 M $\text{ZnCl}_2/\text{Zn}(\text{CH}_3\text{COO})_2$ was widely applied as the electrolyte for rechargeable Zn–air batteries [12]. In 2000s, the flexible rechargeable Zn–air batteries with polymer electrolytes consisting of polymer and KOH were proposed to satisfy the demands for flexible electronics [29]. The researches on polymer with the ability to bind water have been intensely explored to achieve long lifespan [30]. Recently, a large number of researches about bifunctional electrocatalysts involving both the ORR and OER, including single-atom catalysts, carbon materials, perovskite oxide, spinel oxide, and transition-metal compounds, have been proposed for reducing the potential gap between charge and discharge of Zn–air batteries, thus achieving high-energy efficiency [31–33]. With the emergence of high-efficient bifunctional oxygen electrocatalysts, the commercialization process of rechargeable Zn–air batteries has been accelerated. The timeline of the development of Zn–air batteries is shown in Figure 1.2.

Up to now, the rechargeable Zn–air batteries have made great progress in the field of electric vehicles. The Electric Fuel company in Israel developed a mechanically rechargeable Zn–air battery for electric buses, showing an energy density of 200 Wh kg^{-1} , which is reaching up to the advanced Li-ion batteries at present [34, 35]. In addition, the Mercedes Benz cars with mechanically rechargeable Zn–air batteries could be able to drive up to 425 km on one charge [36]. The key technology for mechanical rechargeable Zn–air battery is the recovery of zinc anode after deep discharge. To overcome the issues of zinc replacement, a zinc paste circulating Zn–air battery with specific energy density of 228 Wh kg^{-1} was designed by Metallic Power Inc., while the spent zinc paste was reduced to fresh zinc paste outside the battery [37]. Other companies, including EOS Energy Storage, ZincNyx Energy Solutions, and Fluidic Energy, also contributed to the development of

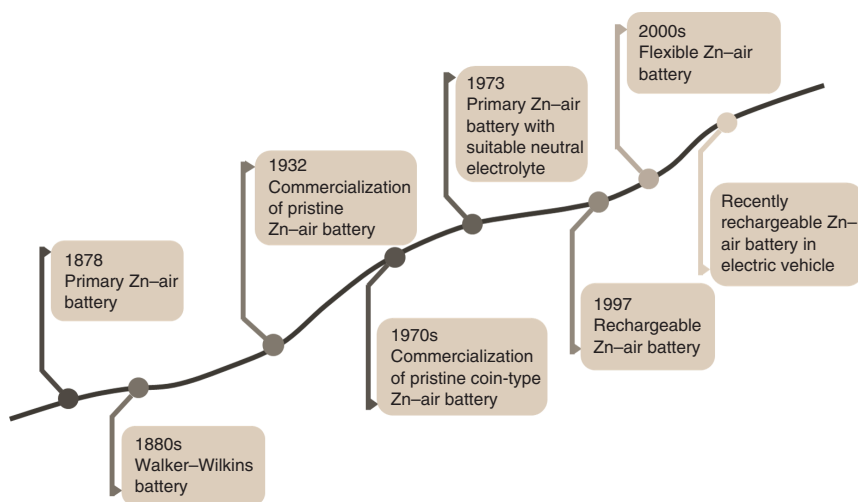


Figure 1.2 Timeline of the development of Zn–air batteries.

Zn–air batteries in practical applications [38]. In addition to electric vehicles, the Zn–air battery could also be applied in wearable devices, unmanned aerial vehicles, communication base stations, electric bicycles, etc.

1.3 Structure and Principle of Zn–Air Batteries

Generally, Zn–air battery is regarded as an alkaline fuel cell, which is composed of three main components—air electrode as cathode involving catalytic active layer and gas-diffusion layer, zinc metal as the anode, and porous separator immersed with alkaline electrolytes, such as 6 M KOH mixed with 0.2 M $\text{ZnCl}_2/\text{Zn}(\text{CH}_3\text{COO})_2$ aqueous solution [39, 40]. In detail, a porous separator is also provided to build a physical barrier between cathode and anode to avoid short circuits, while the electrolyte acts as the medium for the transmission of OH^- between anode and cathode [41]. In addition, the gas-diffusion layer is applied to improve the transfer rate of oxygen to catalysts surface, while the catalytic active layer could facilitate the reaction rate between oxygen and OH^- [42]. During electrochemical discharge process, the reduction of oxygen molecules to OH^- occurs by ORR, while reversible OER occurs during OER process [43]. For zinc anode, which served as the counter electrode, the spontaneous chemical reaction between zinc and OH^- occurs to produce ZnO during discharge process, while the ZnO is decomposed to zinc and OH^- during charge process [43]. In general, zinc metal is regarded as the main active species to achieve electric energy output for pristine Zn–air battery, also called Zn–air fuel cell. For the air electrodes with different catalysts, there are three types of Zn–air batteries models, including pristine Zn–air batteries, two-electrode rechargeable Zn–air batteries, and three-electrode rechargeable Zn–air batteries [44], as shown in Figure 1.3. The sandwich structure of cathode/separator/anode for these three typical batteries are same, while the component of catalytic active layer in air cathode is different.

For pristine Zn–air battery, only ORR occurs on air electrode (Figure 1.3a) [45]. The ORR in alkaline electrolyte is a complex reaction process with multielectron-involved elementary reactions. During the ORR process, molecular oxygen, adsorbed on catalysts surface via the bidentate configuration, is reduced to OH^- through a 4-electron pathway (see Eq. (1.1)) [46]. Otherwise, molecular oxygen, adsorbed on catalysts surface via the end-on one oxygen atom coordination mode, is reduced to HO_2^- through a 2-electron pathway (see Eq. (1.2)) [47]. In general, the 2-electron oxygen-reduction pathway, which is usually applied to produce the hydrogen peroxide (H_2O_2), is regarded as the side reaction for 4-electron oxygen-reduction pathway. The 2-electron pathway may cause tremendous energy loss and inferior discharge durability for Zn–air batteries [48]. Therefore, it is desirable to develop ORR catalysts with 4-electron pathway regarding the activity and stability. When evaluating ORR performance, the electron-transfer number also needs to be calculated with the exception of limiting current and half-wave potential [49]. From the 4-electron ORR equation, the consumption of H_2O and production of OH^- occur for the electrolyte, thus causing the increase of local pH values on cathode surface. The equilibrium potential of 4-electron ORR is

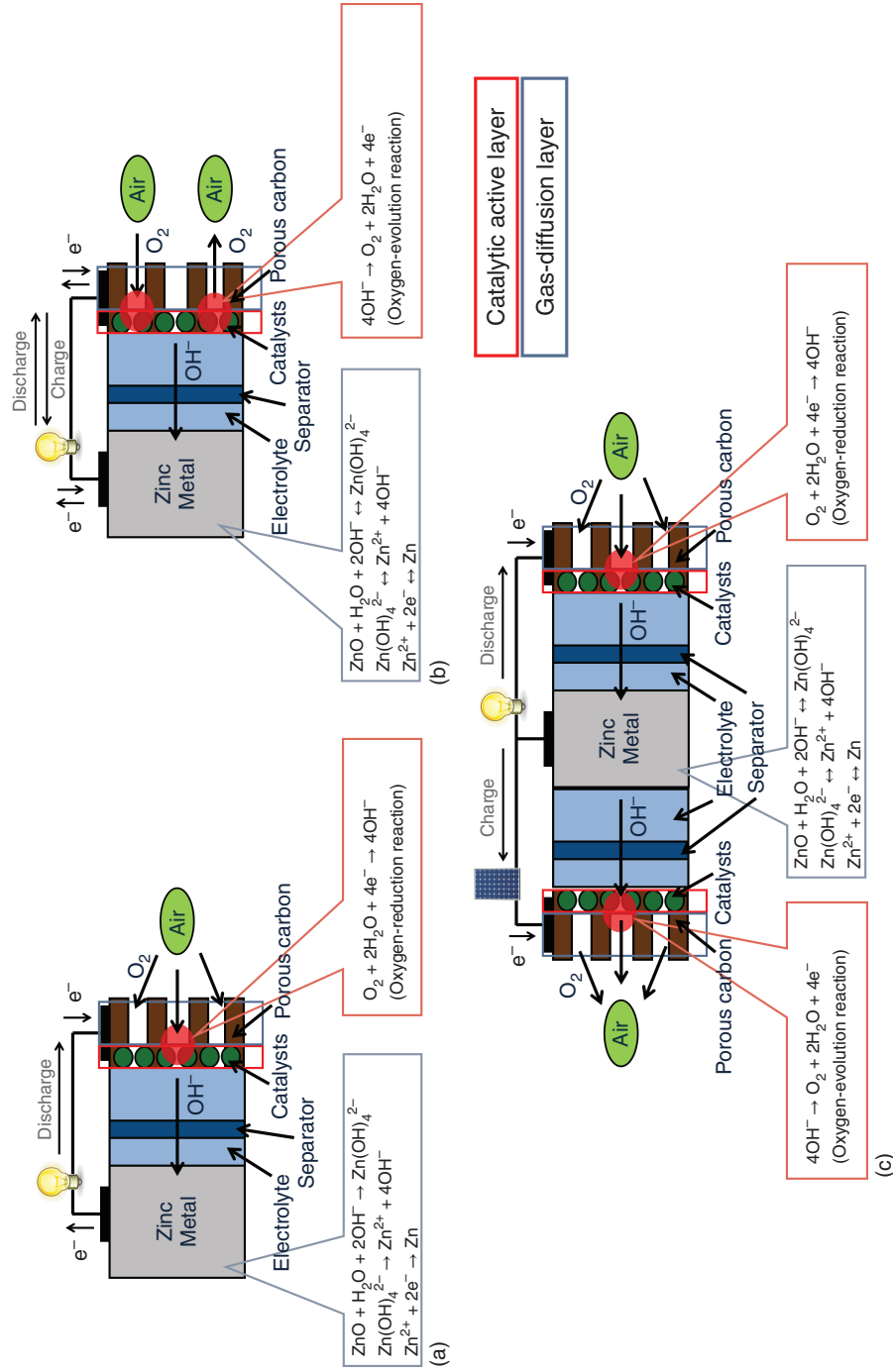
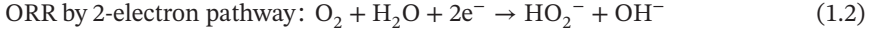
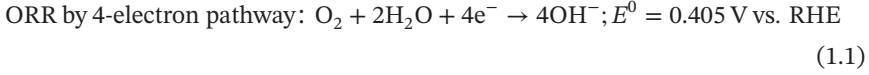


Figure 1.3 Working principle of (a) pristine Zn-air battery, (b) two-electrode, and (c) three-electrode rechargeable Zn-air batteries. Source: Lee et al. [45]/Reproduced with permission of John Wiley & Sons.

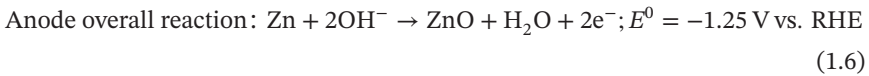
calculated to 0.405 V vs. reversible hydrogen electrode (RHE) based on the redox pair O_2/O^{2-} [50].

Cathode reaction:



During discharge process, the zinc metal first loses two electrons to form the Zn^{2+} , which is further combined with OH^- to form the soluble $Zn(OH)_4^{2-}$ (see Eqs. (1.3) and (1.4)). Finally, the formed $Zn(OH)_4^{2-}$ is decomposed into H_2O , OH^- , and insoluble ZnO at supersaturated $Zn(OH)_4^{2-}$ concentrations on anode surface (see Eq. (1.5)) [51]. When a load is connected to the battery, the generated electron on anode side transfers to air cathode through external circuit, and the 4-electron ORR on air cathode further occurs. From the anode overall reaction equation (see Eq. (1.6)), the consumption of OH^- and production of H_2O occur for the electrolyte [51]. Combined with above cathode reaction, the OH^- would spontaneously transfer from cathode to anode surface during discharge process to overcome the concentration polarization. Therefore, alkaline electrolyte with high ionic conductivity is chosen as the commercial electrolyte. In addition, the distance between cathode and anode is also an important parameter for discharge performance [52]. Based on the redox pair Zn/Zn^{2+} , the equilibrium potential of anode reaction is calculated to be -1.25 V vs. RHE [53].

Anode reaction:



Combining the anode and cathode reaction, the theoretical open-circuit voltage of Zn–air battery should be 1.65 V, where $E^0 = E^0_{\text{cathode}} - E^0_{\text{anode}}$. Generally, the actual open-circuit voltage of Zn–air battery is just 1.4–1.5 V owing to the existence of polarization potential under working conditions [54]. The overall discharge reactions of Zn–air battery is actually the reaction between zinc and oxygen to generate the ZnO (see Eq. (1.7)). In other words, there is just consumption of zinc metal during discharge process. If sufficient zinc metal is provided and the durability of ORR catalysts is excellent, the pristine Zn–air battery could continuously discharge for a long term [55]. Therefore, the mechanical replacement of zinc metal after deep-discharge process with fresh zinc metal could achieve the rechargeability of pristine Zn–air battery. This mechanically rechargeable Zn–air battery has been proved to be a desirable choice for application in electric vehicles [56, 57], and this is discussed in detail later.



For electrochemically rechargeable Zn–air battery, there are two configurations involving two-electrode (Figure 1.3b) and three-electrode (Figure 1.3c) [58]. Generally, two-electrode rechargeable Zn–air battery shows similar configuration to the pristine Zn–air battery. For two-electrode rechargeable Zn–air battery, its catalytic active layer in air cathode mainly consists of bifunctional ORR/OER electrocatalyst, while that of just ORR electrocatalyst for pristine Zn–air battery [59]. Therefore, screening the bifunctional electrocatalysts with both high-efficient ORR and OER activities is necessary for these rechargeable batteries. To assess the bifunctional activity, the potential gap (ΔE) between half-wave potential of ORR and overpotential of OER at 10 mA cm^{-2} is proposed, which is an important parameter for evaluating the bifunctional electrocatalysts [60–62]. In general, lower ΔE value implies higher bifunctional activity [49]. The anodic and cathodic reactions during discharge process are same as that of pristine Zn–air battery mentioned above. During charge process, the OH^- is converted to O_2 on air cathode and the surface ZnO is subsequently reduced to zinc metal on anode. Similarly, the OH^- produced on anode side transfers to cathode side to make up its consumption of OH^- . The generated O_2 is finally transmitted outside through the gas diffusion layer to accomplish the whole discharge/charge process [63]. Unfortunately, the uneven deposition of soluble $\text{Zn}(\text{OH})_4^{2-}$ on zinc anode is observed during charge process, thus inevitably causing the growth of zinc dendrite [64]. In addition to the stability of bifunctional electrocatalyst, zinc dendrite is also a key factor for the cycle life of Zn–air battery [65]. The discussion about the adverse impact of zinc dendrite in Section 1.5.3 is continued.

In general, it is hard to design a bifunctional electrocatalyst with both excellent ORR and OER activities owing to the completely reversible reaction process [55]. The high-efficient ORR or OER catalysts have been developed intensely in the past few years [66, 67]. Although the bifunctional catalysts could be achieved by physical mixing of ORR catalysts with OER catalysts, the random stack of two type of catalysts would affect the actual discharge/charge performance [55]. In addition, numerous ORR catalysts, such as carbon materials, may be decomposed during OER process with high-charging potential [63, 68]. For example, the Zn–air battery with heteroatom-doped carbon materials exhibited excellent discharge performance, including high-power density and high-discharge voltage; however, the power density and discharge voltage are rapidly decreased after first charge process owing to the decomposition of low-crystalline carbon catalyst under high-charge voltage [69]. In addition, the electrolyte turned from clear to yellowish-brown, revealing the electrochemical degradation of carbon-based catalysts [63, 68]. The three-electrode Zn–air battery consisting of air-discharge electrode, air-charge electrode, and zinc anode is proposed to overcome above issues for two-electrode Zn–air battery (Figure 1.3c) [15]. When assembling the three-electrode Zn–air battery, the ORR catalysts and OER catalysts are dropped on gas-diffusion layer to obtain two air electrodes, respectively [70]. Then the two air electrodes form a sandwich structure with zinc metal, while two separators are also inserted between two cathodes and one anode. The air electrode with ORR catalysts and OER catalysts are served as the cathode during discharge and charge process, respectively, and the principle of

discharge and charge for three-electrode Zn–air battery is same as the two-electrode Zn–air battery. During the charge process, the air electrode with ORR catalysts is inoperative, thus avoiding the adverse impact on subsequent discharge performance after charging operation [44]. Although three-electrode Zn–air battery is superior to the two-electrode battery in cycling performance, the tedious configuration would increase the overall weight and volume of Zn–air batteries, which is unfavorable for the gravimetric and volumetric energy density.

As revealed by the overall reactions of Zn–air battery, zinc anode is the main active species to achieve the electric energy output. In many commercial zinc-based dry cells, the gelled mixture of zinc pellets in range of 50–200 mesh is served as the anode [71]. The size of zinc pellets has been proved to be a key factor for Zn–air battery in view of inter-particle contact and reaction activity [72]. In principle, high surface area of zinc pellets means better electrochemical activity. However, the small zinc pellets with high surface energy are easily corroded by the alkaline electrolyte, thus causing serious self-discharge [72]. Dai et al. revealed that the zinc particles with grain size of above 200 mesh show the highest rate capacity owing to the low internal electrical resistance in anode pack [17]. Meanwhile, Metallic Power Inc. reported an electrolytic technique to prepare small dense zinc pellets with size of 0.5–0.6 mm for mechanically rechargeable Zn–air battery, while the spent zinc pellets could be electrochemically reduced to fresh one for further discharge cycles on-site [73]. The zinc pellets are dispersed on alkaline electrolyte to form the liquid electric fuel, which is pumped into the anode side of cell. Moreover, the morphology of zinc metal is also an important influence factor for the discharge energy density of Zn–air batteries [74–76]. For example, the Zn–air battery with fibrous form of zinc shows higher discharge capacity and voltage than commercial zinc particles [77]. For the usage of these zinc powder in Zn–air batteries, the zinc particles or zinc fibers are processed into the rod and plate to form zinc anode for pristine or rechargeable cylindrical and prismatic Zn–air batteries, as shown in Figure 1.4 [77]. This zinc anode always exhibits abundant pore structure for the permeation of alkaline electrolyte, thus achieving fast-discharge reaction. For rechargeable Zn–air battery, after converting the zinc metal to ZnO under desirable depth of discharge

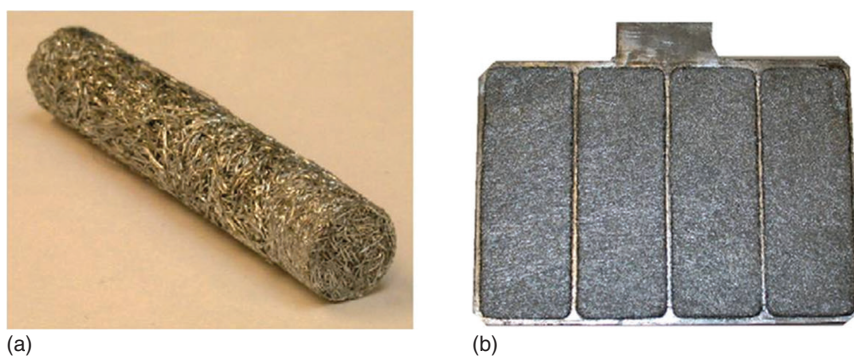


Figure 1.4 The digital photographs of (a) rod form and (b) plate form zinc anode for zinc–air batteries. Source: Zhang [77]/Reproduced with permission of Elsevier.

(DOD), electrochemically reducing the ZnO to fresh zinc electrode is an efficient strategy to realize the rechargeability of Zn–air battery [78].

Aqueous electrolytes, especially alkaline electrolytes, have been widely applied in commercial Zn–air batteries [79]. The alkaline electrolytes show high conductivity, high catalytic activity for both air cathode and zinc anode, and excellent low-temperature activity than neutral electrolyte. The alkaline concentration is an important parameter for Zn–air battery to determine the ionic conductivity [80]. When the alkaline concentration is relatively low, the poor reaction activity and high ion-transfer impedance of electrolyte would be observed, while high-alkaline concentration would also block the ion-transport rate owing to high viscosity of electrolyte [81]. Therefore, there exists optimal alkaline concentration to achieve the highest ionic conductivity. More importantly, KOH electrolyte shows higher ionic conductivity, lower viscosity, and higher oxygen-diffusion coefficients than NaOH and LiOH electrolytes, which have been widely applied in Zn-based batteries [82]. As shown in Figure 1.5a, the 30 wt% KOH electrolyte (about 7 M) shows the highest conductivity of 0.64 S cm^{-1} at room temperature, and the conductivity increases with the temperature [56, 83]. Fortunately, the 30 wt% KOH electrolyte also achieves fairly high conductivity of 0.22 S cm^{-1} when the temperature decreases to -15°C , revealing that the Zn–air battery with alkaline electrolyte could operate in a wide temperature range. In addition to aqueous electrolytes, polymer electrolytes, which

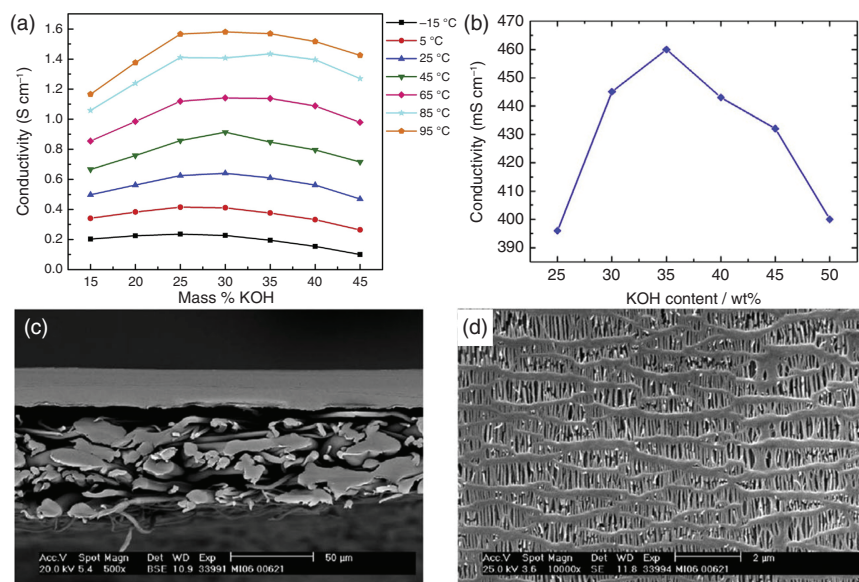


Figure 1.5 (a) The conductivity of alkaline electrolyte under different KOH concentrations and temperatures, Source: See and White [83]/Reproduced with permission of Elsevier., (b) the conductivity of gel polymer electrolyte under different KOH concentrations. Source: Zhang et al. [84]/Reproduced with permission of Elsevier., and the (c) cross section and (d) top-view images of nonwoven separator for Zn–air battery. Source: Kritzer and Cook [85]/Reproduced with permission of IOP Publishing.

are formed by conducting salts and polymers, are designed to eliminate the air cathode flooding for aqueous batteries. In general, the conducting salts is mainly KOH and polymers consists of polyvinyl alcohol (PVA) [86], poly(acrylic acid) (PAA) [87], poly(ethylene glycol) (PEG) [88], polyacrylamide (PAM) [89], and polyacrylate [87]. The ionic conductivity mechanism of polymer is the ionic motion in the chain segment, therefore, constructing the amorphous phase in the polymer above the glass transition temperature (T_g) is beneficial for the ionic conductivity of polymer electrolyte [90]. In addition, PAA-based polymer electrolyte with 35 wt% KOH exhibits high conductivity of 0.46 S cm^{-1} at room temperature (Figure 1.5b) [84], which is even comparable to the aqueous electrolytes. As reported, the polymer electrolyte is a desirable choice for flexible Zn–air batteries owing to its superior flexibility and mechanical strength [79].

The separator, as an electrochemically inactive component in Zn–air battery, is applied to physically isolate the cathode and anode. In general, separator is a critical component for Zn–air battery, which should satisfy the criteria of low ionic and high electrical resistance to allow fast ion transfer between cathode and anode [91, 92]. Moreover, separator should have low-contact angle with aqueous electrolytes, high chemical stability toward the corrosion and oxidation of electrolytes, and high mechanical strength to resist the zinc dendrite attack [13, 92]. Only the separator meeting above requirements can effectively improve the performance of Zn–air battery, including high security, high-discharge capacity, and long-term durability. Nonwoven polymers, such as polypropylene (PP), polyethylene (PE), polyamide (PA), and PVA, have been widely applied as the separator for traditional aqueous alkaline Zn–air batteries [85]. These nonwoven separators always show high porosity of 75%, which could achieve high electrolyte retention and low ionic resistance [85]. At present, laminated nonwoven separators, such as Celgard 5550, with a trilayer structure (PP/PE/PP) as shown in Figure 1.5c,d, while PP and PE layers are respectively applied to maintain the integrity of separator and shut down the battery when thermal runaway, is typically used in commercial coin type of Zn–air batteries [85]. When battery is short circuited, the PE layer would melt under high temperature and further closes the pores to shut down the battery, thus realizing safe operation. Given that the separator is an inactive component for Zn–air battery, its thickness and weight should be exactly controlled when applied for commercial application.

Owing to the low solubility of oxygen in the aqueous electrolyte, the active oxygen mainly diffuses in through the gas-diffusion layer during discharge process, and transfers out through the gas-diffusion layer during charge process to achieve the oxygen exchange between catalyst surface and external atmosphere, not the liquid electrolyte [93]. The charge and discharge reactions mainly occur at the three-phase interface between electrolyte, electrode, and oxygen (Figure 1.6) [39, 43, 94]. During discharge process, the oxygen is first diffused to catalysts surface to form the O_2^* and further reduced to OH^* at the catalysts surface, and then, the OH^- is desorbed from the catalysts surface and diffused to electrolyte, while the electrons required for surface reaction from O_2^* to OH^* are provided by external conductive skeleton [94, 95]. Therefore, porous carbon black is needed in catalytic active layer

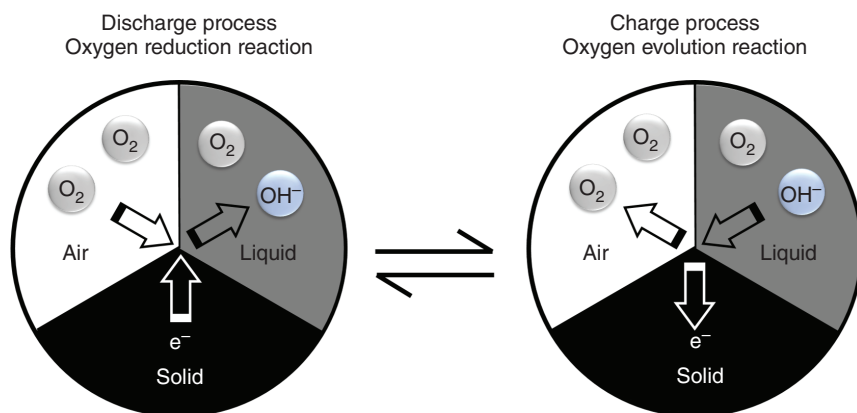
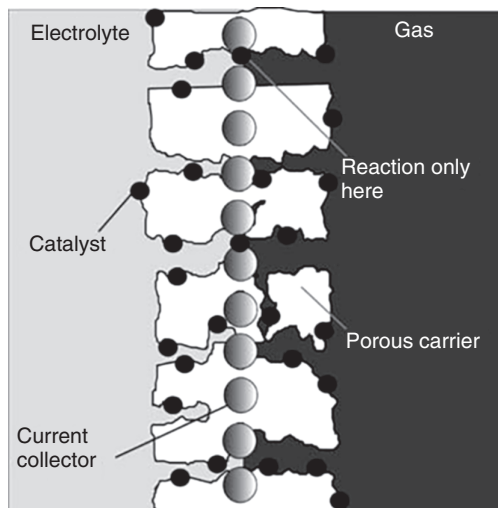


Figure 1.6 Schematic illustration of three-phase interface reaction for discharge and charge process.

considering the electron transfer and oxygen diffusion. The charge process is opposite to the discharge process, in detail, the OH^- absorbed from electrolyte is converted to oxygen through the OER catalysts and the oxygen is diffused outside through the gas-diffusion layer, while the generated electron is transferred from catalysts surface to zinc anode through external conductive skeleton [96]. The distribution of electrolyte and oxygen inside the air cathode determines the transmission distance of reactant and internal resistance, and the area of three-phase interfaces directly determines the active catalytic areas for ORR and OER inside the air cathode. Therefore, the formation of abundant efficient three-phase interfaces inside the air electrode is beneficial for the overall utilization rate of the electrocatalyst, thus improving the charge/discharge performance. If the three-phase interface is damaged, the discharge performance would seriously be decreased owing to trace oxygen in electrolyte is not sufficient to maintain the reaction [40, 97]; in addition, the generated oxygen could not be diffused outside and adhered to on catalysts surface, which isolates the catalysts from direct contact with the electrolyte, thus decreasing the charge performance owing to the catalytic active site is covered [96]. Therefore, maintaining the stability of the three-phase interface during charge/discharge process has also a direct impact on the cycle stability of Zn–air battery.

Based on above discussion about three-phase interface, the structural design of high-efficient air electrode, which accounts for the transfer of oxygen gas, has a great influence on its charge/discharge performance. In general, the hydrophobic air electrode is applied for Zn–air battery to build three-phase transfer interface, as shown in Figure 1.7 [20]. There is a hydrophobic region in air electrode for gas diffusion, and this porous region could serve as the carrier to store the oxygen gas [98]. Owing to the hydrophobic features of the porous carrier, electrolyte cannot fill the unpressurized gas chamber. At present, porous carbon, including carbon fiber, carbon-woven cloth, nonwoven fabric, activated carbon, and acetylene black, and polytetrafluoroethylene (PTFE) are first mixed, and further rolled and hot-pressed into a gas-diffusion layer, in which porous carbon provides gas chamber and PTFE

Figure 1.7 Schematic diagram of air electrode. Source: Harting et al. [20]/Reproduced with permission of Walter de Gruyter GmbH.



guarantees the hydrophobicity [99, 100]. The gas resistance is proposed to evaluate the performance of gas-diffusion layer owing to the oxygen being the critical active species during discharge process [101]. Generally, low gas resistance means fast oxygen-transfer rate during discharge process, which could ensure high-discharge rate performance. In addition, the mechanical strength of gas-diffusion layer should be considered owing to the repeated charge and discharge operations that could damage its inner structure [102]. For the catalytic active layer, the catalysts are hydrophilic to form the electrolyte film on catalysts surface, while the film serves as the depletion layer to achieve the OH^- exchange between catalysts and electrolytes [103]. The core of catalytic active layer is the bifunctional electrocatalyst, which could determine the overall performance of Zn–air battery [16]. In addition, the current collector, such as metal foam and mesh, is introduced between gas-diffusion layer and catalytic active layer to ensure the efficient transfer rate of electrons to or from external circuit [104]. A zigzag structure between the contact faces of gas-diffusion layer and catalytic active layer is formed to achieve continuous transmission network. At the contact interface, the high-efficient air electrode must meet the condition that there is a large amount of gas within the chamber, and building an interconnected channel between the thin electrolyte film and gas chamber is necessary [104]. Therefore, the air electrode must be a thin porous electrode with different hydrophobicity on both sides, in which the hydrophobic side should possess sufficient air holes for the transfer of oxygen to catalysts surface and the hydrophilic side should build enough electrolyte permeation channel for the species exchange between electrolyte and catalysts.

The emergence of miniaturized electronic devices, such as hearing aids, urges researchers to develop long-lasting energy supply. Zn–air batteries with high-energy density, low cost, and stable output voltage show obvious advantages in these electronic devices [105]. Up to now, the coin type of pristine Zn–air battery has been successfully applied as the power supply for hearing aids. As shown in Figure 1.8, coin type of batteries generally consists of the following components—air cathode,

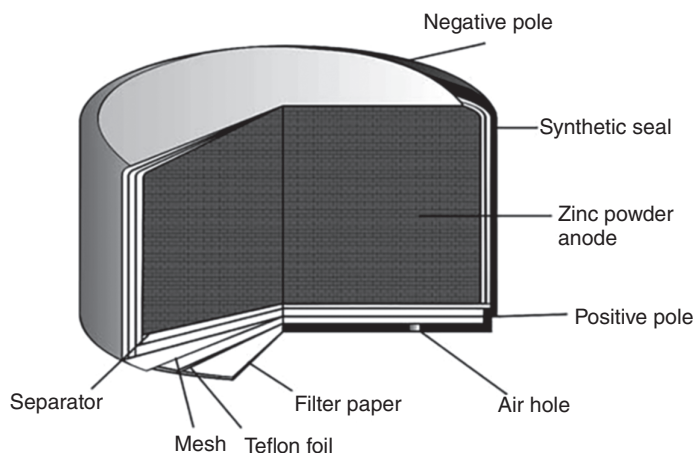


Figure 1.8 Schematic diagram of the coin type of Zn–air battery. Source: Harting et al. [20]/Reproduced with permission of Walter de Gruyter GmbH.

zinc anode, separator, electrolyte, insulating ring, and packaging shell. As previously described, air cathode is composed of catalytic active layer, gas-diffusion layer, and current collector [20]. In this coin type of battery, the waterproof layer (Teflon foil) serves as the gas-diffusion layer to prevent the electrolyte leakage. It is noteworthy that the volume and mass of air cathode could be ignored, while the zinc anode is the main component for this commercial battery owing to the zinc metal being the only consumptive active species, which also determines the discharge capacity of Zn–air battery. In addition, zinc powder rather than zinc foil is used as the anode owing to its large contact area with electrolyte. This type of Zn–air battery just discharges for a long time under low-current density, thus it can only be used in miniaturized electronic devices. To prevent battery aging, the air hole is always sealed by tape, and the tape needs to be removed before use. If the sealing tape is removed, the coin type of battery must be discharged until complete consumption of zinc anode owing to the adverse influence of CO_2 in atmosphere, and the detailed information is discussed in section of 1.5.2.

For electrochemically rechargeable Zn–air battery, the commercialization process has been impeded by the large charging overpotential owing to the inferior catalytic activities for OER electrocatalysts, and its energy efficiency is generally lower than 65% as laboratory reported [31]. In general, low-energy efficiency means low-energy utilization, while the side reactions, such as water electrolysis, would be occurred. Therefore, the high-efficient bifunctional electrocatalysts need further exploration to promote the commercial electrochemically rechargeable Zn–air battery. As previously mentioned, the mechanically rechargeable Zn–air battery is a desirable choice for electric vehicles [106]. Electric Fuel Ltd. has developed a mechanically rechargeable Zn–air battery for electric vehicles from the targets of price, safety, performance, and quick refueling [107]. As shown in Figure 1.9a, a static replaceable anode cassette containing the slurry of zinc particles is covered by isomorphic separator envelope and further embedded into a current collection

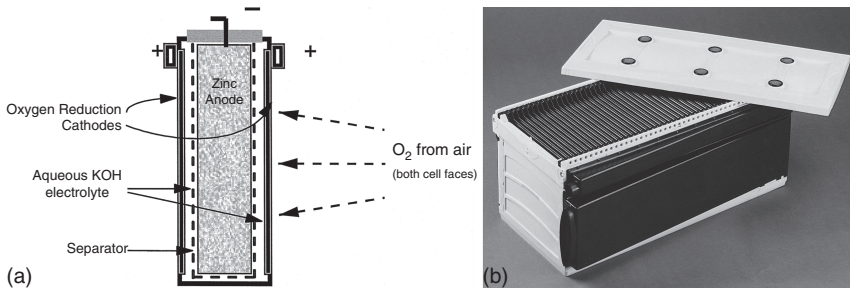


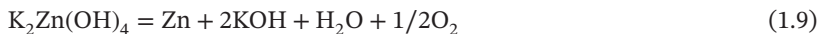
Figure 1.9 (a) Schematic diagram of mechanically rechargeable Zn–air battery by Electric Fuel Ltd. Source: Goldstein et al. [107]/Reproduced with permission of Elsevier. (b) the battery module containing 47 individual Zn–air batteries. Source: Goldstein et al. [107]/Reproduced with permission of Elsevier.

frame which is modified with high-efficient oxygen-reduction catalysts flanked on two sides, while the gap between catalyst layer and anode cassette was filled with potassium hydroxide solution [107]. As discussed above, zinc metal serves as the only electric fuel during discharge process, while exchanging spent electric fuel after deep discharge with fresh electric fuel could achieve charging performance of Zn–air battery, and this process is called refuel or mechanically recharge. Within the anode cassettes, zinc particle with high surface area and high-tapped density is tightly compacted onto a current collector to achieve a robust anode. The high surface area of zinc particles is beneficial for the discharge performance, however, the small zinc particles with high activity would react with electrolyte, thus inevitably causing negative self-discharge. Therefore, the corrosion rate of zinc particles should be controlled by the electrolyte additive to lower the self-discharge rates [108]. The time of refueling process for this type of Zn–air battery is comparable to that of gasoline refueling for fuel vehicle, revealing it could be applied in the field of electric vehicles.

After deep discharge at 80% DOD, the zinc metal is completely oxidized to ZnO based on the overall discharge reaction. The spent electric fuel could be electrochemically recharged outside the Zn–air battery to achieve the regeneration of zinc anode in zinc electrowinning cells. As reported, suitable morphology and size of zinc particles could be obtained at the electrowinning current density of 100–200 mA cm⁻² within the voltage of 2.2 V, which could achieve high-energy efficiency for cycled Zn–air batteries [107]. To achieve regeneration of zinc anode, the residual solid ZnO, which is collected from the dead Zn–air battery after deep discharge, is first dissolved in a KOH solution to obtain the soluble K₂Zn(OH)₄ as following Eq. (1.8):



Then, the soluble K₂Zn(OH)₄ is electrolyzed in a zinc electrowinning cell to regenerate the zinc particles as following Eq. (1.9):



After electrowinning process, the zinc particles are collected and recompact into the current collector frame. Finally, the recycled anode cassettes are inserted into a

fresh separator envelope, and further embedded into the previous current collection frame with original catalysts flanked on two sides, thus realizing a mechanically charging cycle. To achieve the application in electric vehicle, 47 individual Zn–air batteries are constructed into a basic module, as shown in Figure 1.9b [107], while a simple air-cooled thermal management system is inserted in the module casing.

The static ZnO particles would block the contact channels between the remainder of fresh zinc particles and electrolyte, thus preventing further discharge reaction. Therefore, the spent zinc particles and other side products should be cleaned up in time to allow direct contact between fresh zinc metal and electrolyte. Recently, flowing bed is proposed to achieve the regeneration of zinc particles [109], however, the parallel bipolar plate cannot well solve the problem of blocking spent zinc particles. Therefore, a tapered-end structural Zn–air battery with unparallel bipolar plate is designed, while air cathode covered with separator is tightly compacted onto the vertical plate, and its front and side sectional views are exhibited in Figure 1.10 [110]. During discharge process, alkaline electrolyte containing zinc pellets continuously falls to the hopper through a narrow opening (<3 mm), and further flows from the top of cell to bottom. The catalytic active region is on the top of cell, while it mainly serves as the reservoir for the zinc pellets. When reacted with oxygen, the zinc pellets continuously decreased in size and meanwhile flowed downwards by their own gravity. After deep discharge, the mixture of solid ZnO, side product, unreacted zinc metal, and electrolyte flowed out from bottom of the cell. Significantly, replacing the spent electrolyte mixture with the fresh electric fuel containing electrolyte and zinc pellets could be accomplished by pump to achieve refueling.

The spent electrolyte is pumped to a storage tank for further regeneration by applying a combined electrochemical and mechanical treatment. In detail, slight mossy zinc metal is electrochemically deposited on a porous nickel substrate under a constant current density and flow speed. Most regenerated zinc particles (about 80%) could not be adhered to the porous substrate owing to their own weight [110]. These regenerated zinc particles are further collected at the bottom of the electrolysis. Subsequently, the collected zinc particle is mechanically pressed into a cylindrical pellet, which is mixed with alkaline electrolyte and readded into

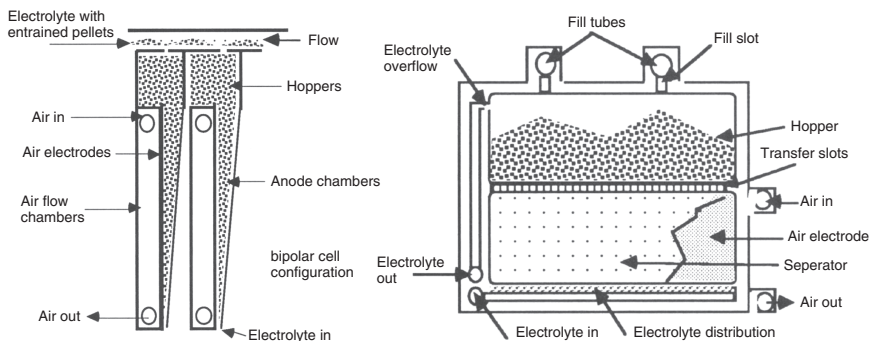


Figure 1.10 Schematic diagram of Zn–air battery with a tapered-end structure. Source: Cooper et al. [110]/Reproduced with permission of SAE International.

the storage tank as the fresh electric fuel. As a result, the tapered-end structural Zn–air battery with air electrode area of 250 cm^2 and hopper volume of 150 cm^3 exports high-specific energy of 525 Wh and high-peak power of 125 W , revealing great potential in electric vehicle [110].

Although above tapered-end structure shows obvious superiority in zinc regeneration, the existence of many gaps between individual cells would increase the weight and volume of overall battery module. Metallic Power Inc. designed an advanced zinc fuel cell to make full use of the vacant space tapered-end structure [73]. A pellet distributor manifold is developed for this cell to decrease the uneven split-flow of electric fuel. For this zinc fuel cell, a slightly inclined anode plate and a vertical air electrode is developed, while the electric fuel is pumped from the top to bottom and the air is permeated from the side. Almost all spaces in cell are utilized as the active sites involving the discharge reaction. During discharge process, the electric fuel consisting of alkaline electrolyte and zinc pellets pours into the cell via channel Q1, and further zinc pellets are dropped out of the electric fuel and into zinc anode bed, in which the zinc pellets are gradually oxidized to a small size as it moves to the bottom of the bed, as shown in Figure 1.11 [73]. The spent electrolyte with ZnO particles, side products, and unreacted zinc pellets flows out the bed from the mesh at the bottom of cell and further returns to the reservoir tank via channel Q2, while excess fresh electrolyte flows out through channel Q3 and finally returns back to the fuel tank. For the regeneration of electric fuel, a spouted bed electroplating method is proposed to recycle the zinc pellets on-site. In detail, a large number of metal pins are embedded in a nonconductive substrate to form the regenerator, while the discrete zinc particles are first grown on the metal pins and further a scraper is mechanically rotated to remove the discrete zinc particles from metal pins surface. Similarly, the regenerated zinc pellets are mixed with fresh alkaline electrolyte to serve as the cyclic electric fuel.

Essentially, the mechanically rechargeable Zn–air battery is a primary battery, while after applying ingenious structural design, the charging ability of primary Zn–air battery could be achieved by quickly replacing spent zinc metal to fresh one [111]. For this battery, only oxygen-reduction catalysts are needed for air electrodes,

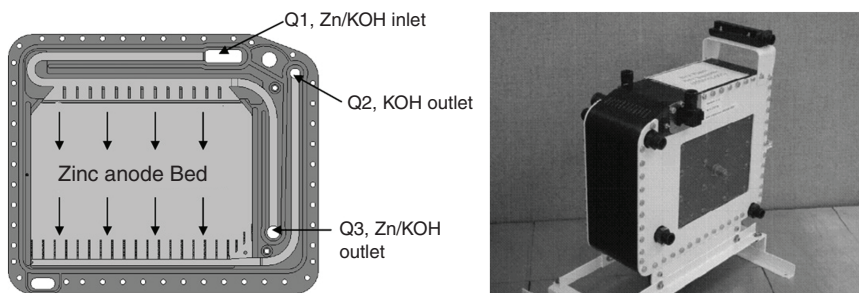


Figure 1.11 Schematic diagram of zinc fuel cell frame by Metallic Power Inc. Source: Smedley and Zhang [73]/Reproduced with permission of Elsevier.

therefore, their life-span is obviously higher than the electrochemically rechargeable Zn–air battery. Up to now, these mechanically rechargeable Zn–air batteries have been successfully applied in electric vehicles, especially electric buses [26]. However, the volume of these mechanically rechargeable Zn–air batteries is largely owing to the use of accessory equipment, such as reservoir tank and regenerator. In contrast, the electrochemically rechargeable Zn–air battery is a desirable choice for electric vehicles owing to its simple structure [112]. Searching for OER and bifunctional ORR/OER catalysts with high catalytic performance and durability are the critical tasks for electrochemically Zn–air batteries.

1.4 Evaluation of Zn–Air Batteries

The performance evaluation of Zn–air battery mainly includes the following parameters – specific capacity density, specific energy density, power density, and charge/discharge performance [113]. It is noteworthy that above parameters have two different references, including weight of electrode and overall battery system, while the reference of electrode weight is mainly used to evaluate the performance of electrode, and the reference of overall battery system weight is applied to assess the practical application value.

1.4.1 Specific Capacity Density

The capacity of a battery refers to the total amount of electricity generated by complete discharge under given conditions and time, while theoretical capacity means the electricity generated by complete consumption of active species [114]. Therefore, the capacity density mainly refers to the discharge performance of Zn–air battery. The calculation formula of theoretical capacity is concluded as follows [115]:

$$C_0 = n \times F \times m_0 \quad (1.10)$$

where n represents the number of electrons involved in the reaction, m_0 represents the consumption mass of active species, and F represents the Faraday constant. There are two types of specific capacity—gravitational-specific capacity represents the amount of electricity released by a unit mass of battery system or active species ($C_1 = C_0/m$, m means the mass of active species or battery system); and volumetric-specific capacity represents the amount of electricity released by a unit volume of battery system or active species ($C_1 = C_0/V$, V means the volume of active species or battery system). In general, zinc metal is the main active species for Zn–air batteries while the oxygen is obtained from atmosphere, and the gravitational-specific capacity is widely used to evaluate the discharge performance of Zn–air battery. Here, we use the mass consumption of zinc metal to determine the gravitational-specific capacity. The theoretical gravitational-specific capacity could be calculated as following formula [115]:

$$\begin{aligned} C_1 &= C_0/m_0 = n \times F \\ &= 2 \times 96\,485 \text{ (C mol}^{-1}\text{)}/3600\text{(C Ah}^{-1}\text{)}/65\text{(g mol}^{-1}\text{)} = 824 \text{ mAh g}_{\text{zn}}^{-1} \end{aligned} \quad (1.11)$$

Therefore, the theoretical-specific capacity density of Zn–air battery is $824 \text{ mAh g}_{\text{Zn}}^{-1}$. The actual specific capacity density means the actual generated electricity under certain discharge conditions, which is calculated by following formula [116]:

$$C = I \times T / m_0 \quad (1.12)$$

where I represents the discharge current (mA), T represents the discharge time (h), and m_0 represents the mass consumption of zinc metal (g). Generally, the actual specific capacity density is lower than theoretical value owing to the inevitable side reaction of zinc anode which will be discussed below in detail. The voltage–time curve is first obtained and then converted to voltage–specific capacity density curves based on the formula (1.12). As shown in Figure 1.12, the voltage–specific capacity density curves could be distinguished into three regions, which are as follows [55]:

- (1) Polarization region with immediate drop of voltage after imposing the discharge current.
- (2) Potential decay region with the slow decaying of voltage.
- (3) Zinc passivation region with rapid drop of voltage at the end of discharge process.

The polarization region at the initial stage is mainly caused by the large polarization voltage on both cathode and anode surface once imposing the discharge current, while the polarization voltage on air cathode surface plays a leading role [117]. The rapid drop voltage at zinc passivation region is attributed to the high-current density on residual fresh zinc metal at the end of discharge process. In addition, the specific capacity density decreases with the increase of discharge current density as shown in Figure 1.12, while the discharge voltage is also decreased owing to the large IR drop under high-current density. The value of specific capacity density represents the utilization rate of zinc anode in alkaline electrolyte, which is highly related to

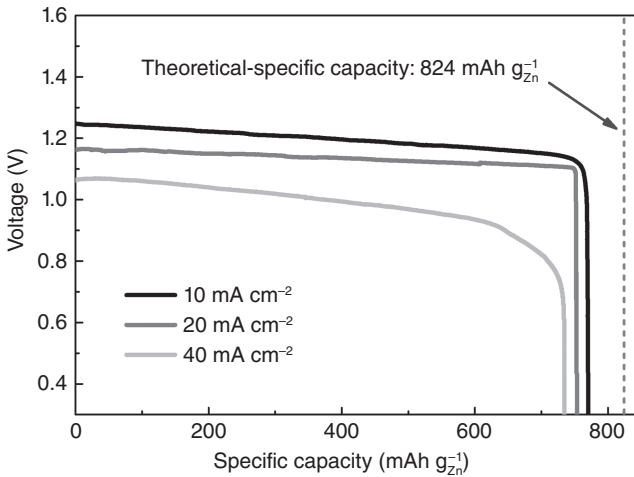


Figure 1.12 Galvanostatic discharge voltage–capacity curves for a typical Zn–air battery with carbon-based catalyst at different current densities. Source: Lu et al. [55]/Reproduced with permission of John Wiley & Sons.

catalytic activity of air cathode and side reaction in zinc anode [118]. Therefore, the specific capacity density based on the mass consumption of zinc metal is a critical evaluating indicator for the discharge performance of Zn–air battery, which is always applied to compare with other reported works about Zn–air batteries with different catalysts [31]. The specific capacity density based on the total mass of battery is another evaluating indicator for the practical application potential. In addition to designing high-performance ORR catalysts, the protection of zinc anode to inhibit the side reaction is also a desirable strategy to improve the specific capacity density owing to the side reaction, such as formation of zinc dendrite, zinc corrosion, and zinc passivation, consumes the fresh zinc metal to inactivated one [119]. After deep discharge, replacing the fresh zinc as anode could recover the discharge performance of Zn–air battery. The discharge-specific capacity density declines after repeatedly mechanical recharging for pristine Zn–air battery owing to the decay of catalytic activity [55]. For electrochemically rechargeable Zn–air batteries, the specific capacity density is generally determined by controlling the DOD, including discharge/charge times and current density [120].

1.4.2 Specific Energy Density

Specific capacity density, directly related to current density and discharge time, is an important parameter to estimate the utilization rate of active zinc metal, while the discharge voltage polarization is not considered. Generally, the discharge platform of Zn–air battery is extraordinarily stable, which is declined with increasing the discharge current density owing to the existence of potential polarization. The discharge voltage is affected by both the air cathode and zinc anode, while the air cathode plays a dominant effect [121]. Therefore, energy density is proposed to measure the actual energy output, and specific energy density refers to the energy output per unit mass or volume of active species or battery system, which is an extremely important evaluating indicator for practical application of battery. Up to now, the gravitational-specific energy density based on the mass consumption of zinc metal is widely applied to evaluate the catalytic activity of air cathode [122]. The theoretical-specific energy density could be calculated as following formula [123]:

$$\begin{aligned} W_1 &= C_1 \times E^\theta \\ &= 824 \text{ (mAh g}^{-1}\text{)} \times 1.65 \text{ (V)} = 1350 \text{ Wh kg}_{\text{Zn}}^{-1} \end{aligned} \quad (1.13)$$

where C_1 represents the theoretical-specific capacity density ($\text{mAh g}_{\text{Zn}}^{-1}$), and E^θ represents the theoretical open-circuit voltage (V). The theoretical-specific energy density of Zn–air battery is $1350 \text{ Wh kg}_{\text{Zn}}^{-1}$. Actually, the specific energy density is far less than the $1350 \text{ Wh kg}_{\text{Zn}}^{-1}$, given the working voltage of Zn–air battery is just 1.2–1.3 V owing to the large discharge overpotential, which could be calculated by following formula [123]:

$$W = C \times E \quad (1.14)$$

where C represents the discharge-specific capacity density ($\text{mAh g}_{\text{Zn}}^{-1}$), and E represents the working voltage (V). The specific energy density based on the mass

consumption of zinc metal is limited to comparing the discharge performance of the catalyst on Zn–air battery [124]. When compared with other types of batteries, the specific energy density based on the total mass of battery should be provided owing to different working voltages of these batteries. For Zn–air battery, achieving high-energy density based on the total mass of battery pack is the premise of its application in the field of electric vehicles [125]. Up to now, the energy density of mechanically rechargeable Zn–air battery could reach up to 228 Wh kg^{-1} with about 100% DOD, which is comparable to the state-of-the-art Li-ion battery with ternary oxide as cathode [126]. In general, the energy density of electrochemically rechargeable Zn–air battery is lower than that of mechanically rechargeable Zn–air battery owing to its limited DOD (generally less than 40%) [127].

1.4.3 Power Density

The voltage–current curves (also polarization curves) are first obtained from linear sweep voltammetry at a constant current or voltage step. Polarization occurs when the current density increases owing to the electrical resistance near the electrode inevitably enhances [128]. Therefore, the polarization curves represent that the voltage change is strongly associated with the current density change. From the charge/discharge polarization curves, the charge/discharge overpotential at different current densities could be obtained. As shown in Figure 1.13a, the polarization curves are distinguished into three regions, which are as follows [26]:

- (1) Activation loss region with sharp drop of voltage ranging from the open-circuit voltage to first-step voltage.
- (2) Ohmic loss region with the slow drop of voltage.
- (3) Concentration loss region with rapid drop of voltage at high-current density owing to the dominant role for mass-transport effect.

For Zn–air battery, the activation loss region and concentration loss regions with sharp drop of voltage mainly occur in the initial stage and high-current density,

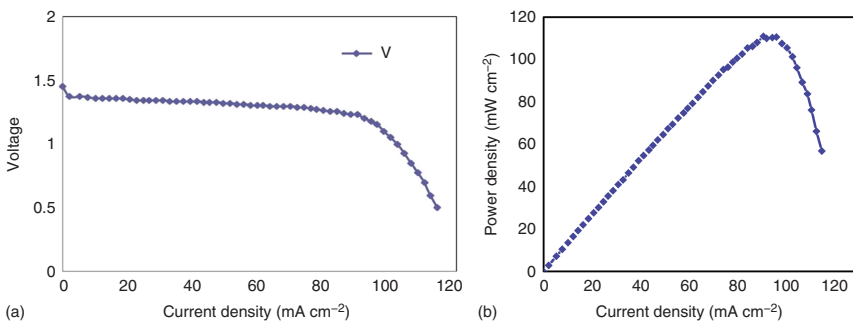


Figure 1.13 (a) The polarization curve and (b) power density curve of a typical Zn–air battery. Source: Sapkota and Kim [26]/Reproduced with permission of Elsevier.

respectively [129]. Therefore, the Ohmic loss region is the choice for normal operation. When operated in Ohmic loss region, Zn–air battery could discharge with a stable voltage.

Power density refers to the output energy available per hour, which is the product of discharge current density and voltage obtained from the polarization curves. Owing to the existence of Ohmic loss, the discharge voltage declines with increasing the current density [130]. Therefore, there exists peak power density for Zn–air battery in the Ohmic loss region. As shown in Figure 1.13b, when peak power density is reached, the power density declines with increasing the current density owing to effects of mass-transport rate and internal resistance [26]. To improve the peak power density, the charge-transfer rate and electronic conductivity during surface reaction should be seriously considered. The charge-transfer rate is mainly dominated by the ORR catalytic activity and oxygen concentration on catalysts surface, and the electron-transfer rate is regulated by the conductive skeleton [63]. Therefore, the peak power density is an efficient evaluating indicator to assess the design structure of air electrodes and catalytic activity of ORR catalysts in practical Zn–air batteries.

1.4.4 Charge/Discharge Performance

Above performance characterization mainly focuses on the discharge process, as for electrochemically rechargeable Zn–air battery, the cycling performance is evaluated by the galvanostatic charge/discharge measurements. In general, the current density and time of discharge and charge process are set to the same values to test the energy efficiency and charge/discharge overpotential [131]. The cycling measurements consists of repeated charge and discharge process. Although the stability of ORR and OER can explain the stability of Zn–air battery to a certain extent, the destruction of ORR catalytic site under OER process with high potential is also a common phenomenon for carbon-based bifunctional catalysts [68]. Therefore, the electrochemical stability of bifunctional catalysts in air cathode is an important factor for the cycling stability of Zn–air battery. Generally, with the increase in cycle times, the change of charge/discharge polarization and energy efficiency represents the cycling stability of Zn–air batteries [49]. The energy efficiency (E_f) and charge/discharge overpotential (ΔE) are applied to assess the charge/discharge performance, and corresponding calculation formulas are listed as follows [132]:

$$E_f = E_d/E_c \quad (1.15)$$

$$\Delta E = E_c - E_d \quad (1.16)$$

where E_d and E_c represent the discharge voltage and charge voltage, respectively. The specific energy is the product of specific capacity and voltage; therefore, the energy efficiency is the ratio of E_d and E_c owing to the same discharge and charge-specific capacity under same current density and time. In addition, the depths of charge and discharge also have a great influence on the cycle performance of Zn–air batteries [127, 133]. During discharge process, the zinc metal is first

dissolved in electrolyte to form the soluble $\text{Zn}(\text{OH})_4^{2-}$, which would cause uneven deposition of zinc during charge process [134]. Therefore, the high depths of charge and discharge would cause low-utilization rate of zinc anode, thus degrading the cycling performance. Up to now, the depths of charge and discharge are relatively lower than 40% for the rechargeable Zn–air battery, which greatly affects the actual energy density [127]. In addition to cycling performance, rate performance is also a critical parameter to test the Zn–air battery. Different from cycling test, rate measurement consists of repeated charge and discharge processes at different current densities [135]. The charge/discharge overpotential increases and energy efficiency declines with improving the current density owing to the existence of large IR drop [135]. Except for the overpotential, the retention rate of energy efficiency under different current densities is also applied to assess the catalytic activity of air electrodes, especially under high-current density.

1.5 Main Issues of Zn–Air Batteries

Although Zn–air battery shows great superiority, there are still many issues for air cathode, electrolyte, and zinc anode. Especially, air cathode, electrolyte, and zinc anode are the main components to determine the performance of Zn–air batteries [45]. Therefore, the existing issues for the three main components need to be emphatically considered to accelerate the commercialization of Zn–air batteries.

1.5.1 Air Cathode

As mentioned above, air electrode mainly consists of catalytic active layer and gas-diffusion layer, while the gas-diffusion layer is composed of porous carbon and PTFE, and the catalytic active layer is composed of ORR/OER catalysts and conductive carbon black [136]. In general, the gas-diffusion layer is hydrophobic and the catalytic active layer is hydrophilic; therefore, the preparation process of air electrodes is extremely cumbersome [42]. The air electrode should satisfy following requirements at the same time—(i) excellent and stable hydrophobicity for gas-diffusion layer ensures fast permeation of oxygen from atmosphere and further promotes discharge reaction; (ii) appropriate hydrophilicity for catalytic active layer ensures that the electrolyte is spread on the catalyst to achieve fast surface reaction; (iii) excellent electronic conductivity ensures that electrons can rapidly transfer out or in during surface reaction. After repeated charge/discharge process, the hydrophobicity of gas-diffusion layer may be destroyed, thus the gas-transmission channel is flooded with aqueous electrolyte [97, 137]. As a result, the discharge performance is seriously affected owing to the low solubility of oxygen in the aqueous electrolyte. In addition, the carbon materials in gas-diffusion layer and catalytic active layer may be decomposed under high-charging voltage, thus causing inferior cycling life-span and rating capacity [63]. Multifunctional air electrode with three-phase species exchange is hard to maintain structural stability, especially after repeated charge/discharge operations. Moreover, the

stability of bifunctional electrocatalysts should be emphatically considered owing to the ORR active site may be damaged at high-charging voltage, as a result, the subsequent discharge performance would seriously descend [63]. When operated at high-current density, a large amount of oxygen is needed for discharge reaction. The oxygen-transport capacity through the gas-diffusion layer cannot meet the consumption rate of oxygen, thus decreasing the power density of Zn–air battery. Although pure oxygen could be directly applied as the active species, the usage of additional equipment and high cost of the compression and storage of oxygen limits its application in portable device [138]. The development of high-performance gas-diffusion layer with ultralow gas resistance and high oxygen selectivity still needs further development.

For rechargeable Zn–air battery, bifunctional electrocatalysts are the critical component for air electrodes to achieve discharge/charge performance. The sluggish ORR/OER catalytic activities lead to high charge/discharge overpotential, thus greatly degrading the energy efficiency of rechargeable Zn–air battery [60, 139]. To understand the relationship between actual working potentials and catalytic activities, the polarization curves of discharge/charge in cathode and anode is schematically illustrated in Figure 1.14 [45]. The equilibrium potential of rechargeable Zn–air battery is 1.65 V as revealed by black line. However, actual working potential is difficult to reach the equilibrium potential owing to the existence of polarization on both the cathode and anode surface. During discharge process, the actual oxygen-reduction potential is far below the equilibrium potential of ORR and the actual oxidation potential is slightly higher than the equilibrium potential. While during charge process, the actual oxygen-evolution potential is far higher than the equilibrium potential of OER and the actual oxidation potential is slightly lower than the equilibrium potential. It is noteworthy that the charge/discharge polarization of Zn–air battery is mainly derived from the ORR and OER in air

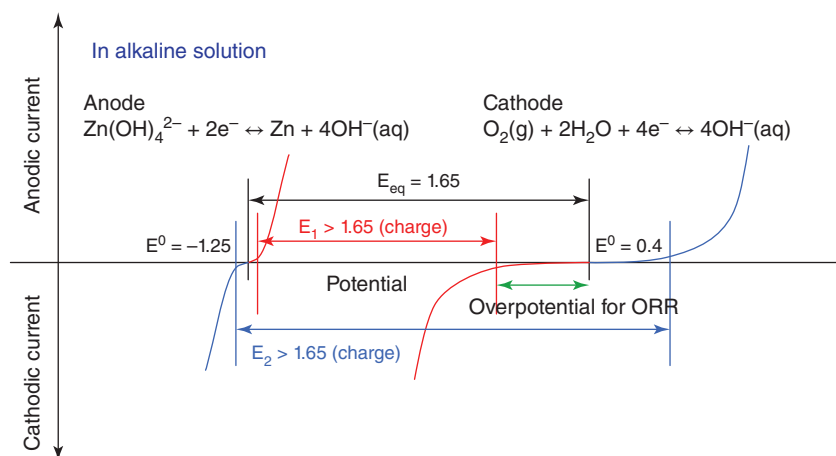


Figure 1.14 Schematic illustration of charge/discharge polarization curves. Source: Lee et al. [45]/Reproduced with permission of John Wiley & Sons.

cathode owing to the polarization in zinc anode is much less than that in air cathode (red line for discharge polarization and blue line for charge polarization). In general, the discharge and charge voltages of Zn–air batteries are usually less than 1.3 V and higher than 1.9 V, respectively, causing large charge/discharge overpotential [140, 141]. To simplify above illustration, the charge/discharge voltage could be concluded as following equation:

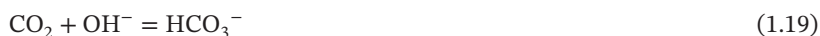
$$\text{Charge process: } E_c = 1.65 - \eta_c - \eta_a - IR \quad (1.17)$$

$$\text{Discharge process: } E_d = 1.65 + \eta_c + \eta_a + IR \quad (1.18)$$

where the E_c and E_d represent actual charging and discharging voltage, η_c and η_a represent cathode and anode overpotential, and IR represents the ohmic drop, respectively. The IR value could be ignored owing to the excellent ionic conductivity of 6 M KOH electrolyte and the overpotential in zinc anode (η_a) could be also ignored. Therefore, the charge/discharge voltages of Zn–air batteries are completely dependent on the overpotential in air cathode. The high charge/discharge overpotential means low-energy efficiency [142]. Up to now, high-performance ORR/OER catalysts has not yet met the needs of practical application in rechargeable Zn–air battery. Although noble metal (Pt, Ru, and Ir) catalysts show superior catalytic activities, their high cost and low durability limit the large-scale application in actual device [55].

1.5.2 Electrolyte

The alkaline electrolytes, such as KOH and NaOH, are widely used in Zn–air batteries to achieve high-reaction activity of zinc anode and air electrode [79]. Generally, the aqueous electrolyte is directly exposed to atmosphere through the porous gas-diffusion layer, thus the evaporation of water easily occurs at high temperature and low humidity of atmosphere. Especially when the atmospheric humidity is less than 60%, the evaporation rate of electrolytes is extremely rapid during long-term cycle [143]. The evaporation of water from electrolyte would cause the precipitation of KOH crystal, thus reducing the ionic conductivity of electrolyte; as a result, the charge/discharge overpotential of Zn–air battery is increased specially at high-current density [144]. In addition, the oversaturated KOH crystal would be precipitated in the gas-diffusion layer, thus blocking the gas-diffusion channel [145]. When operated under low temperature and high humidity of atmosphere, the alkaline electrolyte could absorb water from atmosphere to reduce the electrolyte concentration, which is adverse to the ORR and OER activity. Moreover, owing to the gas-diffusion layer having no selectivity for oxygen gas, the CO_2 could be also transmitted to the gas chamber through the gas-diffusion layer. For alkaline electrolytes, the CO_2 could react with KOH to form the K_2CO_3 and KHCO_3 as following equation [146]:



The carbonate dissolved in electrolyte would increase the viscosity of electrolyte thus reducing its ionic conductivity, and the concentration of OH^- in electrolyte is reduced thus decreasing the ORR/OER catalytic rate in air cathode. Meanwhile, decreasing the OH^- concentration leads to the deposition of ZnO on zinc surface and further improves the resistance [147]. In addition, the solid carbonate is partially crystallized inside the gas-diffusion layer, which would block the oxygen-diffusion channel [145]. As a result, the oxygen reaction efficiency in air electrodes is seriously limited by the oxygen-diffusion rate. Although numerous neutral electrolytes have been developed for Zn–air battery to solve the carbonation of alkaline electrolyte, the inferior reaction activity in both the cathode and anode side is a big problem to be solved for neutral electrolytes [145]. In addition, the neutral electrolyte shows extremely low ionic conductivity, which causes high internal resistance for Zn–air battery [148]. Up to now, no work can achieve that the ionic conductivity of neutral electrolyte is comparable to that of alkaline electrolyte.

The main components of polymer electrolyte consist of KOH, water, and polymer. Similar to aqueous alkaline electrolyte, the evaporation of water and side reaction between KOH and CO_2 are also the main issues for polymer electrolyte [149]. The bound water in polymer chain is easily consumed based on the volatilization and reaction with zinc dendrite [150]. After water volatilizing, the KOH crystal is precipitated on the surface of polymer electrolyte, which would block the ion-transport channels, thus reducing the ionic conductivity. Water is the active species for discharge reaction; therefore, the volatilization of water would break off of discharge reaction. In addition, the formation of carbonate also blocks the ion-transport channels, which is unfavorable for the cycling life-span of polymer Zn–air batteries. In general, the interface between polymer electrolytes in semisolid form and air cathode in solid form should be emphatically considered. For aqueous electrolytes, the electrolyte could permeate into catalytic active layer to improve the ion-transport interface between catalysts and electrolytes, while the ion exchange through the solid–solid interface is hard to achieve for polymer electrolytes [151]. As a result, the high interface transfer impedance leads to high charge/discharge overpotential. Moreover, the ionic conductivity and stability of polymer electrolyte need further improvement.

1.5.3 Zn Anode

In general, the issues for zinc anode are highly associated with the electrolyte. In alkaline electrolyte, zinc metal is active enough to react with OH^- for Zn–air battery [119]. During discharge process, the electrical stripping of zinc metal into electrolyte after losing two electrons is referred to as the zinc corrosion as Eq. (1.21), which is called parasitic reaction [45]. When there are no external loads, the zinc corrosion reaction on anode side spontaneously occurs, and this process is called self-discharge, which would seriously degrade the operation life of Zn–air battery after air electrode accessing the oxygen. The electrons lost by zinc metal may selectively combine with water to form the hydrogen owing to the similar potentials of zinc corrosion (hydrogen evolution) and zinc dissolution [74].

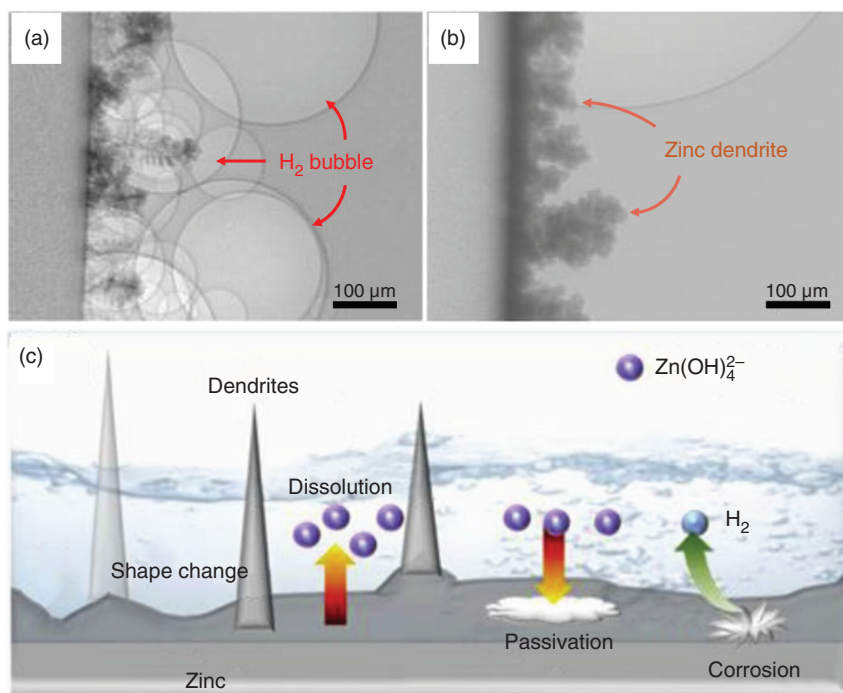
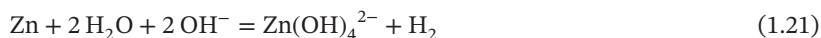


Figure 1.15 Microradiographs of (a) hydrogen bubble and (b) zinc dendrite with galvanostatic plating at 20 and 13 A dm⁻²; Source: Hsu et al. [153]/Reproduced with permission of IOP Publishing., and (c) schematic illustration of possible reaction on zinc electrode. Source: Han et al. [154]/Reproduced with permission of Elsevier.

Generation of by-product hydrogen would seriously decrease the Faraday efficiency of zinc dissolution. As mentioned before, the zinc metal is the only active species to output the electric energy, therefore, the zinc and electrolyte consumption by side hydrogen production reaction during discharge process leads to severe deterioration in the discharge capacity, and this reaction is not reversible [152]. In addition, the generated hydrogen would be tightly adsorbed on the zinc surface owing to the strong adsorption strength, as shown in Figure 1.15a [153]. Abundant hydrogen bubble isolates the ion exchange between zinc anode and electrolyte, which would increase the corresponding anode interface resistance, thus depriving the charge/discharge overpotential of Zn–air battery [74]. Moreover, the package of Zn–air battery would be swelled after accumulation of large amounts of hydrogen inside the battery.



For rechargeable Zn–air battery, the growth of zinc dendrite is an urgent problem to be solved. As mentioned before, the solid ZnO is first reduced to soluble $\text{Zn}(\text{OH})_4^{2-}$ during charge process, and soluble $\text{Zn}(\text{OH})_4^{2-}$ is further reduced to the zinc metal on anode surface. The soluble $\text{Zn}(\text{OH})_4^{2-}$ is randomly distributed near the anode surface owing to uneven distribution of current and potential on zinc

surface and gravity effect of electrolyte [45]. Under the influence of electric field and gravitational field, the uneven deposition of zinc on anode surface unavoidably occurs, thus causing the shape change of zinc anode and forming a rough anode surface [155]. As charging progresses, the soluble $\text{Zn}(\text{OH})_4^{2-}$ preferentially adsorbed and reduced on the small dendrite tip with sharp end structure based on the tip discharge principle, thus continuously forming the abhorrent zinc dendrite on those shape end. Generally, zinc dendrite is regarded as the inactivated species, also called dead zinc, and it will fall off from the anode surface when it grows to a certain length, as a result, the actual discharge capacity of Zn–air battery is far less than the theoretical capacity of 824 mAh g^{-1} owing to the generation and loss of inactive zinc dendrite [156]. As shown in Figure 1.15b, the length of zinc dendrite could grow up to $150 \mu\text{m}$, while the thickness of separator is just $50 \mu\text{m}$ (Figure 1.5c), therefore, zinc dendrites can pierce the separator and contact with the air cathode, thus causing the short circuit of Zn–air battery [153]. Moreover, compare with pure zinc metal, zinc dendrite with high surface energy could further promote the generation rate of undesirable hydrogen bubbles on anode surface. The adverse effects of hydrogen bubbles inside Zn–air batteries have been discussed above. As reported, the growth of zinc dendrite mainly observed in alkaline electrolytes because in which zinc metal shows high electrochemical activity [156]. In addition, the growth rate of zinc dendrite is positively related to the current density, therefore, the problem of zinc dendrite in Zn–air battery is more serious when operated at high-current density.

The passivation of zinc surface is also an inevitable problem for zinc anode in both alkaline and neutral electrolyte [154]. During discharge process, the zinc metal dissolves into electrolyte to form hydroxide. When hydroxide near the zinc surface is oversaturated, the $\text{ZnO}/\text{Zn}(\text{OH})_2$ would be precipitated on the zinc surface for alkaline and neutral electrolyte, as shown in Figure 1.15c [154], respectively. The dense passivation layer prevents further discharge reaction of internal fresh zinc metal, thus decreasing actual discharge capacity and even leading to battery failure. After covering passivation layer, the actual active area of zinc anode decreases, and the real anodic current density increases, further promoting the growth of ZnO passivation layer. Moreover, the insulated ZnO layer would decrease the electronic conductivity of zinc anode, thus affecting the rate performance of Zn–air battery [155]. Therefore, the low stripping/plating efficiency of zinc anode arises in alkaline electrolytes given the corrosion, passivation, and dendrite issues. For electrochemically rechargeable Zn–air battery, deep discharge of zinc anode cannot be achieved owing to the zinc skeleton cannot be well maintained after 100% DOD based on above issues on zinc anode. Up to now, the DOD of zinc anode is significantly lower than 40% [127]. Searching for efficient strategies to achieve high DOD is urgently needed for rechargeable Zn–air batteries to realize high-energy density.

Acknowledgments

This work was financially supported by the Start-up Foundation for Introducing Talent of NUIST.

References

- 1 Tarascon, J.M. and Armand, M. (2001). *Nature* 414: 359.
- 2 Chu, S., Cui, Y., and Liu, N. (2016). *Nature Materials* 16: 16.
- 3 Dunn, B., Kamath, H., and Tarascon, J.-M. (2011). *Science* 334: 928.
- 4 Lu, Q., Zou, X., Ran, R. et al. (2019). *Journal of Materials Chemistry A* 7: 22463.
- 5 Choi, J.W. and Aurbach, D. (2016). *Nature Reviews Materials* 1: 16013.
- 6 Kamat, P.V. (2019). *ACS Energy Letters* 4: 2757.
- 7 Slater, M.D., Kim, D., Lee, E., and Johnson, C.S. (2013). *Advanced Functional Materials* 23: 947.
- 8 Chen, J., Naveed, A., Nuli, Y. et al. (2020). *Energy Storage Materials* 31: 382.
- 9 Liu, Y., Li, B., Cheng, Z. et al. (2018). *Journal of Power Sources* 395: 439.
- 10 Manthiram, A., Fu, Y., Chung, S.-H. et al. (2014). *Chemical Reviews* 114: 11751.
- 11 Lee, D.U., Xu, P., Cano, Z.P. et al. (2016). *Journal of Materials Chemistry A* 4: 7107.
- 12 Zhong, Y., Xu, X., Wang, W., and Shao, Z. (2018). *Batteries & Supercaps* 2: 272.
- 13 Zou, X., Lu, Q., Zhong, Y. et al. (2018). *Small* 14: 1801798.
- 14 Blurton, K.F. and Sammells, A.F. (1979). *Journal of Power Sources* 4: 263.
- 15 Cai, X., Lai, L., Lin, J., and Shen, Z. (2017). *Materials Horizons* 4: 945.
- 16 Yi, J., Liang, P., Liu, X. et al. (2018). *Energy & Environmental Science* 11: 3075.
- 17 Li, Y. and Dai, H. (2014). *Chemical Society Reviews* 43: 5257.
- 18 Zhao, S., An, H., and Chen, S. (1998). *Journal of Power Sources* 76: 218.
- 19 Maiche, L. (1878). French Patent 127069.
- 20 Harting, K., Kunz, U., and Turek, T. (2012). *Zeitschrift für Physikalische Chemie* 226: 151.
- 21 Heise, G.W. and Schumacher, E.A. (1932). *Transactions of the Electrochemical Society* 62: 383.
- 22 Cohn, G. and Ein-Eli, Y. (2010). *Journal of Power Sources* 195: 4963.
- 23 Xu, N., Liu, Y., Zhang, X. et al. (2016). *Scientific Reports* 6: 33590.
- 24 Li, L. and Manthiram, A. (2016). *Advanced Energy Materials* 6: 1502054.
- 25 Jindra, J., Mrha, J., and Musilova, M. (1973). *Journal of Applied Electrochemistry* 3: 297.
- 26 Sapkota, P. and Kim, H. (2009). *Journal of Industrial and Engineering Chemistry* 15: 445.
- 27 Allebrod, F., Chatzichristodoulou, C., Mollerup, P.L., and Mogensen, M.B. (2012). *International Journal of Hydrogen Energy* 37: 16505.
- 28 Atwater, T.B. (1998). *IEEE Aerospace and Electronic Systems Magazine* 13: 36.
- 29 Malone, E., Berry, M., and Lipson, H. (2008). *Rapid Prototyping Journal* 14: 128.
- 30 Yang, C.C. and Lin, S.J. (2002). *Journal of Power Sources* 112: 497.
- 31 Meng, F.L., Liu, K.H., Zhang, Y. et al. (2018). *Small* 14: 1703843.
- 32 Liu, X., Zhang, G., Wang, L., and Fu, H. (2021). *Small* 17: 2006766.
- 33 Ren, S., Duan, X., Liang, S. et al. (2020). *Journal of Materials Chemistry A* 8: 6144.

- 34 Goldstein, J.R. and Koretz, B. (1998). Ongoing tests of the Electric Fuel/sup (R)/ zinc-air battery for electric vehicles. *Proceedings of the Conference 13th Annual Battery Conference on Applications and Advances*, 16.
- 35 Koretz, B., Harats, Y., Goldstein, J.R., and Korall, M. (1996). The electric fuel™ zinc-air mechanically rechargeable battery system for electric vehicles. In: *New Promising Electrochemical Systems for Rechargeable Batteries* (ed. V. Barsukov and F. Beck), 143. Dordrecht: Springer Netherlands.
- 36 Dell, R.M. (2000). *Solid State Ionics* 134: 139.
- 37 Riezenman, M.J. (2001). *IEEE Spectrum* 38: 55.
- 38 Fu, J., Cano, Z.P., Park, M.G. et al. (2017). *Advanced Materials* 29: 1604685.
- 39 Pan, J., Xu, Y.Y., Yang, H. et al. (2018). *Advancement of Science* 5: 1700691.
- 40 Davari, E. and Ivey, D.G. (2018). *Sustainable Energy & Fuels* 2: 39.
- 41 Kim, H.-W., Lim, J.-M., Lee, H.-J. et al. (2016). *Journal of Materials Chemistry A* 4: 3711.
- 42 Yu, J., Li, B.-Q., Zhao, C.-X. et al. (2020). *Advanced Materials* 32: 1908488.
- 43 Zhou, T., Zhang, N., Wu, C., and Xie, Y. (2020). *Energy & Environmental Science* 13: 1132.
- 44 Shinde, S.S., Lee, C.-H., Sami, A. et al. (2017). *ACS Nano* 11: 347.
- 45 Lee, J.-S., Kim, S.T., Cao, R. et al. (2011). *Advanced Energy Materials* 1: 34.
- 46 Liu, Z.X., Li, Z.P., Qin, H.Y., and Liu, B.H. (2011). *Journal of Power Sources* 196: 4972.
- 47 Bu, Y., Wang, Y., Han, G.-F. et al. (2021). *Advanced Materials* 33: 2103266.
- 48 Lee, J.-S., Lee, T., Song, H.-K. et al. (2011). *Energy & Environmental Science* 4: 4148.
- 49 Lu, Q., Guo, Y., Mao, P. et al. (2020). *Energy Storage Materials* 32: 20.
- 50 Li, S., Zhou, X., Fang, G. et al. (2020). *ACS Applied Energy Materials* 3: 7710.
- 51 Stock, D., Dongmo, S., Janek, J., and Schroeder, D. (2019). *ACS Energy Letters* 4: 1287.
- 52 Zhao, Z., Yu, W., He, Y. et al. (2021). *Journal of the Electrochemical Society* 168: 100510.
- 53 Dirkse, T.P. and Hampson, N.A. (1972). *Electrochimica Acta* 17: 387.
- 54 Guo, Y., Yuan, P., Zhang, J. et al. (2018). *ACS Nano* 12: 1894.
- 55 Lu, Q., Yu, J., Zou, X. et al. (2019). *Advanced Functional Materials* 29: 1904481.
- 56 Xu, M., Ivey, D.G., Xie, Z., and Qu, W. (2015). *Journal of Power Sources* 283: 358.
- 57 Li, Y. and Lu, J. (2017). *ACS Energy Letters* 2: 1370.
- 58 Zhang, J., Zhao, Z., Xia, Z., and Dai, L. (2015). *Nature Nanotechnology* 10: 444.
- 59 Zhang, M., Dai, Q., Zheng, H. et al. (2018). *Advanced Materials* 30: 1705431.
- 60 Wang, X.R., Liu, J.Y., Liu, Z.W. et al. (2018). *Advanced Materials* 30: 1800005.
- 61 Peng, S., Han, X., Li, L. et al. (2018). *Advanced Energy Materials* 8: 1800612.
- 62 Niu, W., Li, Z., Marcus, K. et al. (2018). *Advanced Energy Materials* 8: 1701642.
- 63 Lu, Q., Zou, X., Liao, K. et al. (2020). *Carbon Energy* 2: 461.
- 64 Chen, P., Wu, Y., Zhang, Y. et al. (2018). *Journal of Materials Chemistry A* 6: 21933.
- 65 Chen, X., Zhou, Z., Karahan, H.E. et al. (2018). *Small* 14: 1801929.

- 66 Hu, C. and Dai, L. (2016). *Angewandte Chemie International Edition* 55: 11736.
- 67 Jamesh, M.-I. and Sun, X. (2018). *Journal of Power Sources* 400: 31.
- 68 Song, S., Li, W., Deng, Y.-P. et al. (2020). *Nano Energy* 67: 104208.
- 69 Huang, L.-B., Zhao, L., Zhang, Y. et al. (2021). *Chemical Engineering Journal* 418: 129409.
- 70 Wang, X., Sunarso, J., Lu, Q. et al. (2019). *Advanced Energy Materials* 10: 1903271.
- 71 Caramia, V. and Bozzini, B. (2014). *Materials for Renewable and Sustainable Energy* 3: 28.
- 72 Thangavel, S., Chen, P.-T., Yan, W.-M. et al. (2020). *International Journal of Energy Research* 44: 11883.
- 73 Smedley, S.I. and Zhang, X.G. (2007). *Journal of Power Sources* 165: 897.
- 74 Lee, S.-M., Kim, Y.-J., Eom, S.-W. et al. (2013). *Journal of Power Sources* 227: 177.
- 75 Ma, H., Li, C., Su, Y., and Chen, J. (2007). *Journal of Materials Chemistry* 17: 684.
- 76 Yang, C.C. and Lin, S.J. (2002). *Journal of Power Sources* 112: 174.
- 77 Zhang, X.G. (2006). *Journal of Power Sources* 163: 591.
- 78 Parker, J.F., Chervin, C.N., Nelson, E.S. et al. (2014). *Energy & Environmental Science* 7: 1117.
- 79 Chen, P., Zhang, K., Tang, D. et al. (2020). *Frontiers in Chemistry* 8: 372.
- 80 Xu, H., Fang, J., Guo, M. et al. (2010). *Journal of Membrane Science* 354: 206.
- 81 Pei, P., Wang, K., and Ma, Z. (2014). *Applied Energy* 128: 315.
- 82 Egan, D.R., de Leon, C.P., Wood, R.J.K. et al. (2013). *Journal of Power Sources* 236: 293.
- 83 See, D.M. and White, R.E. (1997). *Journal of Chemical & Engineering Data* 42: 1266.
- 84 Zhang, Z., Zuo, C., Liu, Z. et al. (2014). *Journal of Power Sources* 251: 470.
- 85 Kritzer, P. and Cook, J.A. (2007). *Journal of the Electrochemical Society* 154: A481.
- 86 Lewandowski, A., Skorupska, K., and Malinska, J. (2000). *Solid State Ionics* 133: 265.
- 87 Zhu, X.M., Yang, H.X., Cao, Y.L., and Ai, X.P. (2004). *Electrochimica Acta* 49: 2533.
- 88 Pal, B., Yasin, A., Kunwar, R. et al. (2019). *Industrial and Engineering Chemistry Research* 58: 654.
- 89 Tan, M.J., Li, B., Chee, P. et al. (2018). *Journal of Power Sources* 400: 566.
- 90 Gadjourova, Z., Andreev, Y.G., Tunstall, D.P., and Bruce, P.G. (2001). *Nature* 412: 520.
- 91 Deimede, V. and Elmasides, C. (2015). *Energy Technology* 3: 453.
- 92 Sato, Y., Kanda, M., Niki, H. et al. (1983). *Journal of Power Sources* 9: 147.
- 93 Antoine, O., Bultel, Y., Ozil, P., and Durand, R. (2000). *Electrochimica Acta* 45: 4493.
- 94 Wang, Y., Cao, Q., Guan, C., and Cheng, C. (2020). *Small* 16.
- 95 Wang, Y., Zou, Y., Tao, L. et al. (2019). *Nano Research* 12: 2055.

- 96 He, Y., Shang, W., Ni, M. et al. (2022). *Chemical Engineering Journal* 427: 130862.
- 97 Lee, D., Kim, H.-W., Kim, J.-M. et al. (2018). *ACS Applied Materials & Interfaces* 10: 22210.
- 98 Maja, M., Tosco, P., and Vanni, M. (2001). *Journal of the Electrochemical Society* 148: A1368.
- 99 Park, S., Lee, J.-W., and Popov, B.N. (2012). *International Journal of Hydrogen Energy* 37: 5850.
- 100 Giorgi, L., Antolini, E., Pozio, A., and Passalacqua, E. (1998). *Electrochimica Acta* 43: 3675.
- 101 Cindrella, L., Kannan, A.M., Lin, J.F. et al. (2009). *Journal of Power Sources* 194: 146.
- 102 Zhou, Y., Jiao, K., Du, Q. et al. (2013). *International Journal of Hydrogen Energy* 38: 12891.
- 103 Wilson, M.S. and Gottesfeld, S. (1992). *Journal of Applied Electrochemistry* 22: 1.
- 104 Nitta, I., Himanen, O., and Mikkola, M. (2008). *Electrochemistry Communications* 10: 47.
- 105 Tan, P., Chen, B., Xu, H. et al. (2019). *Applied Catalysis B: Environmental* 241: 104.
- 106 Chau, K.T. and Wong, Y.S. (2001). *Energy Conversion and Management* 42: 1059.
- 107 Goldstein, J., Brown, I., and Koretz, B. (1999). *Journal of Power Sources* 80: 171.
- 108 Jo, Y.N., Kim, H.S., Prasanna, K. et al. (2014). *Industrial and Engineering Chemistry Research* 53: 17370.
- 109 Huh, T., Savaskan, G., and Evans, J.W. (1992). *Journal of Applied Electrochemistry* 22: 916.
- 110 Cooper, J.F., Fleming, D., Hargrove, D. et al. (1995). *SAE Transactions* 104: 2785.
- 111 Wang, K., Pei, P., Ma, Z. et al. (2014). *Journal of Power Sources* 271: 65.
- 112 Cano, Z.P., Banham, D., Ye, S. et al. (2018). *Nature Energy* 3: 279.
- 113 Guo, Y., Chen, Y.-N., Cui, H., and Zhou, Z. (2019). *Chinese Journal of Catalysis* 40: 1298.
- 114 Wu, M., Zhang, G., Wu, M. et al. (2019). *Energy Storage Materials* 21: 253.
- 115 Wei, T., Li, Q., Yang, G., and Wang, C. (2019). *Advanced Energy Materials* 9: 1901480.
- 116 Liu, C., Zuo, P., Jin, Y. et al. (2020). *Journal of Power Sources* 473: 228604.
- 117 Qiu, C., He, G., Shi, W. et al. (2019). *Journal of Solid State Electrochemistry* 23: 1887.
- 118 Zhang, H., Liu, X., Li, H. et al. (2021). *Angewandte Chemie International Edition* 60: 598.
- 119 Hao, J., Li, X., Zhang, S. et al. (2020). *Advanced Functional Materials* 30: 2001263.
- 120 Luo, M., Zhao, Z., Zhang, Y. et al. (2019). *Nature* 574: 81.
- 121 Mainar, A.R., Iruin, E., Colmenares, L.C. et al. (2018). *Journal of Energy Storage* 15: 304.

- 122 Rahman, M.A., Wang, X., and Wen, C. (2013). *Journal of the Electrochemical Society* 160: A1759.
- 123 Zheng, J.P., Liang, R.Y., Hendrickson, M., and Plichta, E.J. (2008). *Journal of the Electrochemical Society* 155: A432.
- 124 Shang, W., Yu, W., Tan, P. et al. (2019). *Journal of Materials Chemistry A* 7: 15564.
- 125 Jin, Y., Liu, K., Lang, J. et al. (2020). *Joule* 4: 262.
- 126 Savaskan, G., Huh, T., and Evans, J.W. (1992). *Journal of Applied Electrochemistry* 22: 909.
- 127 Parker, J.F., Nelson, E.S., Wattendorf, M.D. et al. (2014). *ACS Applied Materials & Interfaces* 6: 19471.
- 128 Zheng, X., Wu, J., Cao, X. et al. (2019). *Applied Catalysis B: Environmental* 241: 442.
- 129 Shaegh, S.A.M., Nguyen, N.-T., and Chan, S.H. (2010). *Journal of Micromechanics and Microengineering* 20: 105008.
- 130 Srinivasan, V. and Newman, J. (2004). *Journal of the Electrochemical Society* 151: A1517.
- 131 Li, Y., Zhong, C., Liu, J. et al. (2018). *Advanced Materials* 30: 1703657.
- 132 Yamamura, T., Watanabe, N., and Shiokawa, Y. (2006). *Journal of Alloys and Compounds* 408: 1260.
- 133 Guena, T. and Leblanc, P. (2006). How Depth of Discharge Affects the Cycle Life of Lithium-Metal-Polymer Batteries. *INTELEC 06 – 28th International Telecommunications Energy Conference*.
- 134 Cao, Z., Zhuang, P., Zhang, X. et al. (2020). *Advanced Energy Materials* 10: 2001599.
- 135 Chen, S., Zhao, L., Ma, J. et al. (2019). *Nano Energy* 60: 536.
- 136 Huang, H., Zhang, W.K., Li, M.C. et al. (2005). *Journal of Colloid and Interface Science* 284: 593.
- 137 Tran, C., Yang, X.-Q., and Qu, D. (2010). *Journal of Power Sources* 195: 2057.
- 138 Al Shaqsi, A.Z., Sopian, K., and Al-Hinai, A. (2020). *Energy Reports* 6: 288.
- 139 Su, C.-Y., Cheng, H., Li, W. et al. (2017). *Advanced Energy Materials* 7: 1602420.
- 140 Han, X., Wu, X., Zhong, C. et al. (2017). *Nano Energy* 31: 541.
- 141 Cui, Z., Fu, G., Li, Y., and Goodenough, J.B. (2017). *Angewandte Chemie International Edition* 56: 9901.
- 142 Liu, X., Wang, L., Yu, P. et al. (2018). *Angewandte Chemie International Edition* 57: 16166.
- 143 Mainar, A.R., Leonet, O., Bengoechea, M. et al. (2016). *International Journal of Energy Research* 40: 1032.
- 144 Zhang, Y., Qin, H., Alfred, M. et al. (2021). *Energy Storage Materials* 42: 88.
- 145 Sun, W., Wang, F., Zhang, B. et al. (2021). *Science* 371: 46.
- 146 Zhou, Y., Pan, J., Ou, X. et al. (2021). *Advanced Energy Materials* 11: 2102047.
- 147 Hosseini, S., Abbasi, A., Uginet, L.-O. et al. (2019). *Scientific Reports* 9: 14958.
- 148 Shu, X., Yang, M., Tan, D. et al. (2021). *Materials Advances* 2: 96.
- 149 Deavin, O.I., Murphy, S., Ong, A.L. et al. (2012). *Energy & Environmental Science* 5: 8584.

- 150 Huang, Y., Li, Z., Pei, Z. et al. (2018). *Advanced Energy Materials* 8: 1802288.
- 151 Yu, C., Ganapathy, S., Van Eck, E.R.H. et al. (2017). *Nature Communications* 8: 1086.
- 152 Li, H., Ma, L., Han, C. et al. (2019). *Nano Energy* 62: 550.
- 153 Hsu, P.-C., Seol, S.-K., Lo, T.-N. et al. (2008). *Journal of the Electrochemical Society* 155: D400.
- 154 Han, C., Li, W., Liu, H.K. et al. (2020). *Nano Energy* 74: 104880.
- 155 Liang, P., Yi, J., Liu, X. et al. (2020). *Advanced Functional Materials* 30: 1908528.
- 156 Zhao, Z., Fan, X., Ding, J. et al. (2019). *ACS Energy Letters* 4: 2259.